E+A Galaxies and the Formation of Early Type Galaxies at z∼0 [1]

Yujin Yang, Ann I. Zabludoff, and Dennis Zaritsky

Steward Observatory, University of Arizona, Tucson, AZ 85721

yyang@as.arizona.edu, azabludoff@as.arizona.edu, dennis@as.arizona.edu

Tod R. Lauer

National Optical Astronomy Observatories, Tucson, AZ 85726

lauer@noao.edu

J. Christopher Mihos[2]

Department of Astronomy, Case Western Reserve University, 10900 Euclid Ave, Cleveland, OH 44106

hos@burro.astr.cwru.edu

ABSTRACT

E+A galaxies, whose spectra have deep Balmer absorption lines but no significant [OII] emission, are the best candidates for an evolutionary link between star-forming, gas-rich galaxies and quiescent, gas-poor galaxies. Yet their current *morphologies* are not well known. We present *HST*/WFPC2 observations of the five bluest E+A galaxies ($z \sim 0.1$) in the Zabludoff et al. sample to study whether their detailed morphologies are consistent with late-to-early type evolution and to determine what drives that evolution. The morphologies of four galaxies are disturbed, indicating that a galaxy-galaxy merger is at least one mechanism that leads to the E+A phase.

Two-dimensional image fitting shows that the E+As are generally bulge-dominated systems, even though at least two E+As may have underlying disks. In the Fundamental Plane, E+As stand apart from the E/S0s mainly due to their high effective surface brightness. Fading of the young stellar population and the corresponding increase in their effective radii will cause these galaxies to migrate toward the locus of E/S0s. E+As have profiles qualitatively like those of normal power-law early-type galaxies, but have higher surface brightnesses. This result provides the first direct evidence supporting the hypothesis that power-law ellipticals form via gas-rich mergers. In total, at least four E+As are morphologically consistent with early-type galaxies.

We detect compact sources, possibly young star clusters, associated with the galaxies. These sources are much brighter ($M_R \sim -13$) than Galactic globular clusters, have luminosities consistent with the brightest clusters in nearby starburst galaxies, and have blue colors consistent with the ages estimated from the E+A galaxy spectra (several 10^8 yr). Further study of such young star cluster candidates might provide the elusive chronometer needed to break the age/burst-strength degeneracy for these post-merger galaxies.

Subject headings: galaxies: evolution — galaxies: interactions — galaxies: starburst — galaxies: star clusters — galaxies: stellar content

---

1. Introduction

If galaxies evolve morphologically from late to early types, then some may be now changing from star-forming, gas-rich, disk-dominated objects into quiescent, gas-poor spheroidals. Spectroscopic surveys have identified at least one set of candidates for such a transformation: "E+A" galaxies[1], whose spectra have deep Balmer absorption lines but no significant [OII] emission, indicating that star formation ceased abruptly in these galaxies within the last $\sim$ Gyr. In general, E+A galaxies lack significant amounts of HI gas (Chang et al. 2001) and have hot, pressure-supported kinematics (Norton et al. 2001), suggesting that these galaxies are indeed evolving — somehow — from late to early types. However, we do not yet know whether their current *morphologies* are consistent with late-to-early type evolution or what drives E+A evolution.

While the mechanism (or mechanisms) that causes galaxies to pass through an E+A phase is not understood, there are several clues. First, E+A spectra suggest a recent burst of star formation that required the rapid consumption or dispersal of a gas reservoir. Second, although they were first studied in distant clusters (Dressler & Gunn 1983), E+As — at least at low redshifts ($z \sim 0.1$) — lie mostly in low density environments (Zabludoff et al. 1996; Quintero et al. 2003). Third, in low-resolution POSS images, some E+As have features suggestive of tidal tails (Zabludoff et al. 1996). Could E+As be the result of disk galaxy mergers, which are both common in the field and known to enhance star formation? In the merger hypothesis, E+As are further along the "Toomre sequence" (Toomre, A. 1977) and thus more relaxed than systems like the Antennae, whose morphology and kinematics are in such disarray that it is nearly impossible to constrain its endproduct. E+As may thus teach us considerably more about the endpoints of galaxy-galaxy mergers.

We cannot test this picture of E+A formation, or whether the E+A phase is a bona fide late-to-early type transition, without detailed morphological information. Simulations predict that well-evolved major mergers have a hybrid morphology, including fading, low surface brightness tidal tails at large radii, a more relaxed spheroid-dominated core, and a population of young star clusters (Barnes 1988; Barnes & Hernquist 1996; Ashman & Zepf 1992; Mihos & Hernquist 1994). Identifying such low surface brightness or small scale features, even at low redshifts, requires spatial resolution on the order of 100 pc and low sky background levels. Therefore, Hubble Space Telescope imaging of nearby E+As is required.

In this paper, we present the detailed *HST*/WFPC2 morphologies of the five bluest E+A galaxies in the Zabludoff et al. (1996) sample. We review the sample and the data reduction methods in §2. We describe the qualitative morphologies of these galaxies in §3.1, discussing the observed tidal features and the implications for E+A origin. We address the question of whether E+As are consistent with evolution into early types by fitting two-dimensional, surface brightness models to each image and deriving structural parameters such as bulge-to-disk ratio, effective radius, and central surface density (§3.2). In §3.4, we examine the color gradients in the E+As and compare them with the expectations from disk merger models. We compare the results with the fundamental plane for early type galaxies and with the surface brightness profiles of the nearby elliptical galaxies in §3.5 and §3.6, respectively. In §3.7, we search for star clusters in the E+As and ask whether their properties are consistent with late-to-early type galaxy evolution. We discuss the implications of our results for higher redshift galaxy surveys in §3.8, cautioning that bulge-to-disk decompositions, quantitative measures of asymmetry, and tests to uncover tidal features may mislead. Section 4 summarizes our results.

---

[1]Because their spectra are a superposition of a young stellar population (represented by A stars) and an old population (characterized by K stars), these galaxies became known as "E (for elliptical) + A" galaxies (Dressler & Gunn 1983) or, more straightforwardly, "K+A" or "k+a" galaxies (Franx 1993; Dressler et al. 1999; Poggianti et al. 1999).

2.   Observations and Data Reduction

Our *HST* imaging sample is a subset of the 20 nearby E+A galaxies[2] that were spectroscopically identified from 11,113 galaxy spectra in the Las Campanas Redshift Survey (LCRS) with redshifts between 0.07 and 0.18 (Zabludoff et al. 1996). These E+As are selected by requiring that their spectra have strong Balmer absorption features (average equivalent width $\langle H \rangle$ of Hβ, Hγ and Hδ > 5.5Å) and little if any [OII] emission (EW[OII] < 2.5 Å). Three-quarters of the E+As in the sample are in the field, well outside rich cluster environments. The number of each E+A (e.g., EA1) is from Zabludoff et al. (1996) and increases with increasing 4000Å break (D_{4000}) strength. D_{4000} is related to the galaxy's color — bluer galaxies have smaller D_{4000}. EA1 through EA5, the focus of our *HST* study, have the smallest D_{4000}'s, and therefore are more dominated by the young stellar population than the other E+As. This dominance can arise either because they have had the most recent or strongest bursts. For the remainder of this paper, we refer to each galaxy by its assigned number. Table 1 summarizes the basic data of five galaxies: coordinates, redshift, and environment. Throughout this paper, we assume $H_0 = 70$ km s^{-1} Mpc^{-1}, $\Omega_M = 0.3$, and $\Omega_\Lambda = 0.7$.

We obtained high resolution images of the five nearby ($z \sim 0.08 - 0.12$) E+A galaxies with the *Hubble Space Telescope* Wide Field Planetary Camera 2 (WFPC2). Because our sample is at relatively low redshift (typically $z \sim 0.1$, for which $0.5'' = \sim 1$ kpc), it is possible to study the LCRS sample in ways that are not possible for the more classic E+As discovered in distant clusters. We take advantage of this benefit to obtain spatially-resolved spectroscopy (Norton et al. 2001) and sub-kpc imaging here. We observed the sample using the F702W ($\lambda_{\rm eff} = 6997$Å) and F439W ($\lambda_{\rm eff} = 4292$Å) filters and obtained three CR-split 700s exposures for each object. Stacked images were generated by summing the three individual images for each galaxy and filter. The pointing was identical for each image, so no shifting or interpolation was required. We rejected CR events by comparing deviant pixels within the stack to a WFPC2 noise model.

We adopt photometric zero points of the *HST*/WFPC2 from Holtzman et al. (1995) after correcting for the gain=7.0 and the nominal infinite aperture. Our values are the same as given in the *HST Data Handbook*. For the Planetary Camera, F439W and F702W magnitude zero points are 20.884 and 22.428, respectively. We adopt Galactic extinction corrections from Schlegel et al. (1998), assuming an $R_V = 3.1$ extinction curve. $A_{\rm F702W}$ and $A_{\rm F439W}$ are calculated from the relative extinction table in the Appendix (Schlegel et al. 1998). The value for F439W is not available in the Appendix, so we use the extinction appropriate for the Landolt B magnitude.

To compare the magnitudes of galaxies within certain filters across a range of redshifts, or to photometric models, we apply K-corrections. In principle, the K-correction can be calculated by using the spectral energy distribution (SED) of an object with full spectral coverage and high S/N. Unfortunately, flux-calibrated spectra with full spectral coverage and high S/N are not available for our sample. The SEDs of E+As strongly depend both on the stellar mass formed during the starburst and on the time elapsed since the burst. To account for this variation in stellar populations, we examine both extremes — a pure A type and a pure K type stellar spectrum. We use A dwarf and K giant templates from the Gunn-Stryker spectrophotometric atlas (Gunn & Stryker 1983), which covers the wavelength range 3130 to 10800 Å. We artificially redshift the template spectra to $(1 + z)$ and measure the magnitude differences in the F702W and F439W filters using the CALCPHOT routine within the IRAF/SYNPHOT package. In the F702W band the difference between the corrections for the two populations is within $\sim 0.19 - 0.31$ magnitudes. In contrast, the difference in the

---

[2]One (EA20) of the original 21 galaxies turned out to be misclassified as an E+A due to noise in the region of one of the spectral line diagnostics (Norton et al. 2001).

corrections is larger than 0.62 magnitudes for F439W because the F439W filter band includes the Balmer jump. A slight shift of the spectra can cause a large change in measured brightness. We list both sets of corrections in Table 3, but adopt the correction calculated for an A star with the justification that these are the bluest, most A-like, of the E+As in the Zabludoff et al. (1996) sample. Because the K correction is the major source of uncertainty in our error budget, the global photometric quantities, especially colors, possibly harbor significant systematic errors. The sense of any relative colors within a galaxy is not affected, although the numerical values may be.

3. Results and Discussion

The *HST* images provide a wealth of information on the small and large scale structure of these galaxies. With the goal of understanding the origin of the E+A phenomenon and into what these systems will evolve, we investigate the morphologies of these systems, their color profiles, their location on the Fundamental Plane (Jorgensen et al. 1996) of elliptical galaxies, and their relationship to "core" and "power-law" ellipticals (Faber et al. 1997). We also discover a population of associated point sources (possibly young star clusters). Finally, we review the implications of our results, obtained for low-redshift E+As, for the identification and study of such systems at higher redshifts. The reader is referred to Tables 2-5 for a summary of the quantitative results discussed in this section.

3.1. Morphologies: First Impressions

Figure 1 shows the WFPC2 mosaic and PC images of our five E+A galaxies at different contrast levels. The full mosaic images ($80'' \times 80''$) are in the left column. The center of each E+A is located in the PC, which is in the upper right corner of each mosaic. Tidal features that extend into the other CCDs are evident in EA1-3. The middle and right columns contain the F702W ($24'' \times 24''$) and F439W ($12'' \times 12''$) PC images, respectively, on a logarithmic flux scale. *HST*/WFPC2 observations are relatively insensitive in the bluer band so that the signal in the F439W images typically extends out only to ~ 3 kpc, 25% of the red coverage, and even there it is of low signal-to-noise.

These five E+As exhibit a variety of morphologies ranging from a highly complex system (EA1) to what could visually be classified as a barred S0 galaxy (EA5), even though they have been uniformly selected using spectroscopic criteria, i.e., "k+a" type spectra from the LCRS.

EA1 stands apart from the other four E+As. It is composed of two components that are separated spatially by ~ 3 kpc and another companion with a projected separation of 14 kpc (assuming the companion is at the redshift of EA1). The association is supported by an asymmetric feature emanating from the companion that could be tidal material and a faint bridge that appears to connect it to EA1.

EA2 and EA3 also exhibit highly disturbed morphologies, although EA3 could be visually classified as a normal face-on spiral galaxy in the low contrast PC image. This ambiguity in visual classification is discussed in more detail in §3.8. EA2 has tidal tail that extends to at least 50 kpc.

EA4 and EA5 appear less disturbed, although EA4 has somewhat irregular outer isophotes, some lopsidedness (in the F439W filter image), and shell-like structures closer to the center that are visible in the PC image. The mechanism or mechanisms responsible for the spectral E+A phenomenon produce a variety of morphologies. Whether all of these systems will evolve into a somewhat more homogeneous population

— for example, early-type galaxies — is yet unclear.

3.2.   Morphologies : Bulge-Disk Decompositions

While EA2-5 appear to have significant spheroidal components, EA3 and EA4, at least, also seem to have a flattened, or perhaps disk-like, morphology. Understanding the fate of these systems requires a quantitative estimate of the relative importance of the dynamically hot and cold stellar components.

Measuring the surface brightness profile for asymmetric, disturbed systems is challenging. To mitigate potential systematic problems, we use two different algorithms. First, to obtain photometric parameters, r_e and μ_e, we use the two-dimensional image fitting algorithm GALFIT (Peng et al. 2002) designed to extract structural parameters directly from the galaxy image. GALFIT assumes a two-dimensional model profile for the galaxy. The functional form of the models we choose to fit include combinations of an $r^{1/4}$-law, a Sérsic $r^{1/n}$-law, an exponential disk profile, and a spatially constant sky background. We fit the following: the (x, y) position of the center, M_{tot} (the total magnitude of the component), r_e (the effective radius), n (the Sérsic index), q (the axis ratio defined as b/a), the major axis position angle, and c (the diskiness/boxiness index, where $c > 0$ indicates boxy). This index c plays the same role as the $\cos 4\theta$ Fourier coefficient term used often in isophote analysis (Rix & Zaritsky 1995). As GALFIT explores parameter space, it convolves the model image with a point-spread function (PSF) and compares it to the data for each parameter set. The model PSFs are generated for each galaxy by the TinyTim (Krist & Hook 1999) software for the WFPC2. Although convolution is computer intensive, the advantage of the convolution process is that it preserves the noise characteristics of the images and can be applied to low signal-to-noise images.

Because GALFIT begins with a very specific, smooth model, which may be a poor representation of such distorted galaxies, we also measure surface brightness profiles using the IRAF/ELLIPSE algorithm. This approach allows the center, major axis position angle, and ellipticity of each ellipse to change, but does not enforce a model radial profile. To accurately recover the surface brightness profiles without recourse to *ad hoc* models, we applied 20 iterations of Richardson-Lucy deconvolution (Richardson 1972; Lucy 1974). Lauer et al. (1998) showed that the WFPC2 PSF can depress the brightness profile as far out as $0\!\!''\!5$ from the galaxy center. Richardson-Lucy deconvolution allows the intrinsic brightness profile to be recovered to the few percent level down to $r \sim 0\!\!''\!05$, with adequate exposure levels ($S/N \sim 50$ in the galaxy center). With reduced S/N and only 20 deconvolution cycles, the central ($r = 0$) point in the profile may remain slightly-depressed, dependent on the (unknown) intrinsic structure of the galaxy center.

Because EA1 is too disturbed to be reasonably modeled by a simple disk+bulge model, we restrict our analysis to EA2-5. For each galaxy, we fit three different light distributions: $r^{1/4}$ law, $r^{1/n}$ Sérsic law, and $r^{1/4}$ + exponential disk law. For EA2, we do not fit the $r^{1/4}$ + exponential disk law model because we might be seeing this galaxy close to edge-on (see the linear residuals in Figure 2), and it is hard for GALFIT to fit an edge-on disk with an extended tail. The structural parameters and the reduced χ_ν^2's of these three GALFIT models are listed in Tables 4 and 5. With the exception of one case, $1 < \chi_\nu^2 < 2$. These values of χ_ν^2 are somewhat larger than statistically acceptable, due presumably to the presence of asymmetric components, as can be seen in Figure 2.

Of the three profiles we consider, only the Sérsic profile has the flexibility to model either a spheroidal or disk-like system by varying the parameter n. Therefore the best-fit value of n can guide our conclusions about the nature of the galaxy. An exponential disk corresponds to a value of $n = 1$, while the classic de Vaucouleurs profile corresponds to $n = 4$. However, the correspondence between disk system, spheroid, and

n is not quite this simple — fitting Sérsic profiles to SDSS galaxies, Blanton et al. (2003) show a peak at $n = 1$ corresponding to disky systems, but no peak at $n = 4$. Instead, spheroidal systems show a range of n values. This result is further complicated when one factors in differences in radial ranges fit — for example, fitting the inner slope of cuspy power-law ellipticals (e.g., Lauer et al. 1995) will give a much higher n value than will fits at larger radii.

With these caveats in mind, we find that a single Sérsic profile fit yields $n > 5$ for all our galaxies, demonstrating that the light is dominated by a spheroidal component. Indeed, the high values for n indicate a very high concentration of the light, even more than expected for a classic de Vaucouleurs profile. Such high concentrations are consistent with the idea that central starbursts have raised the central luminosity density (e.g., Mihos & Hernquist 1994). For example, in the case of EA4, masking the inner kpc and refitting the Sersic law results in a value of $n = 3.6$, much more typical of a normal elliptical. This is not always the case, however — in EA3, the high Sérsic value persists even when the nucleus is masked out. For EA3 the fitted value ($n = 8.7$) is unusually high compared to normal ellipticals (e.g., Kelson et al. 2000; Graham et al. 2001; Graham 2002). An additional complication to the interpretation of these fits is that, while the light appears to be dominated by a concentrated spheroid, some of the galaxies appear to contain an additional disk-like component that would affect any dynamical model of a merger and its aftermath.

To determine whether these galaxies do indeed contain a disk component, we also fit models with two components. The resulting radial profiles for EA3 and 4 (Figure 3) and the significant decrease in χ^2_ν (an improvement in the fit at the 99% confidence level) demonstrate that a pure spheroid model is not the preferred model for these two systems. To avoid the degeneracies present in fitting disk and bulge simultaneously, we also fit single Sérsic profiles just to the outer parts of the galaxies. Using the effective radii of the bulges calculated from the two-component fit, we mask pixels inside a chosen radius, vary that radius to be $\sim 3 - 5r_e$ and refit a single component. We mark the effective radii and disk scale lengths with circles in Figure 2. For EA3, the best-fit Sérsic indicies are $n = 2.5$, 1.6 and 1.3 for masks corresponding to $3r_e$, $4r_e$, and $5r_e$, respectively. For EA4, we measure $n = 0.93$ and 0.86 when we apply $3r_e$ and $4r_e$ masks, respectively. In both of these cases, the Sérsic index beyond several r_e is as expected for an exponential disk and the fit spans 4 to 5 disk scale lengths. Although we cannot discriminate tidal material from a possible underlying disk, we conclude that in EA3 and EA4 there is material beyond that described by a spheroid and that it is consistent with an underlying disk. EA3 and EA4 appear to be sufficiently relaxed that no significant dynamical evolution is expected, so they may become S0's. We also hypothesize that their progenitors may have included a disk that was significantly heated but not completely destroyed during an intermediate mass ratio merger (e.g., Naab 2000; Bendo & Barnes 2000).

Even though no disturbed tidal structure is apparent in EA5, the modeling is complicated by the presence of a strong bar-like structure. The presence of a bar-like feature suggests an underlying disk. When viewed at the different contrasts in Figure 4, EA5 is composed of at least three distinct components, a extended light distribution in outer part (axis ratio $q \sim 0.8$), a compact and elliptical bar structure ($q \sim 0.4 - 0.5$), and a very bright blue central nucleus. The three-component fit gives the Sérsic index $n = 1.1$ for the central nucleus, $n = 0.5$ (Gaussian) for the bar, and $n = 1.5$ for the outer disk-like region. This three-component Sérsic profile fit (Figure 4) is acceptable and suggests the presence of disk. For mask sizes $2.5r_e$, $3r_e$ and $3.5r_e$, the best fit Sérsic indicies n are 2.0, 1.8, and 1.8, respectively. However, unlike for EA3 and EA4, we do this fit in a limited region and cannot conclude that EA5 has a distinct exponential disk component. The presence of a bar-like feature also suggests an underlying disk.

For the E+As that may contain a disk component, we calculate a bulge-to-total light ratio (B/T) to quantify the relative importance of the bulge and disk-like components. B/T for EA3 and EA4 is 0.56 and

0.62, respectively. These values are larger than the typical B/T for Sa galaxies (0.45) and comparable to the median for S0's (0.63; Kent 1985). Despite the complications of fitting EA5, various modes of fitting the galaxy produce B/T ~ 0.7. Unless the bulge and any underlying disk-like component fade at dramatically different rates, which is unlikely given the relatively weak large-scale population gradients in these galaxies (Norton et al. 2001), the descendants of these galaxies must be early type (S0 or E, if the disk-like material is tidal debris that disperses or collapses onto the central component).

Given the asymmetric features, how reliable are these fits? There are several ways to check the results for possible systematic errors. First, we compare the fitted analytical profiles to the radial surface brightness profiles obtained from the isophote fitting procedure. In Figure 3, we plot the radial surface brightness profiles of a chosen model for each galaxy: $r^{1/4}$ profile for EA2 and EA5, $r^{1/4}$ + exponential disk profile for EA3 and EA4, and the profiles obtained from the isophote fitting. The differences between the data (ELLIPSE) and models (GALFIT) range mostly between ± 0.5 mag/arcsec^2, are not global, and reflect local asymmetric components. Second, we examine the residual images obtained by subtracting the smooth and symmetric models from the data (see Figure 2). In all cases we see evidence for components beyond the bulge + disk model. We then calculate how much light remains in the residual images to quantify the goodness of the fit. The relative asymmetric light — excess (deficit) — within a $10''$ radius is $16(8)\%$, $6(5)\%$, $8(9)\%$, $9(8)\%$ of the symmetric model components for EA2-5, respectively. Most (50% to 80%) of the under(over)subtracted light comes from the central region within $0.5''$, where the even a small amount of fractional deviation from the data can dominate the residual flux over the outer faint parts. Except for EA2, the global under(over)subtractions are roughly the same and localized fluctuations dominate the residuals, so we conclude that our global fits are reliable. In the case with the most residual light (EA2), 24% of the light cannot be explained by a symmetric model and the positive residuals dominate all over the galaxy. Therefore, we cannot exclude the possibility that we are looking right along the interaction plane (the tidal debris are quite linear). The point sources near the E+A bulges in the residual images are discussed in §3.7.

3.3. Morphologies: Asymmetric Components

So far we have fit symmetric smooth models with moderate success, but have found that asymmetric features are quite common in our sample. Asymmetry, in particular lopsidedness, has been used to measure disturbances in local "normal" disk galaxies (Rix & Zaritsky 1995; Zaritsky & Rix 1997) and correlates with recent star formation (Zaritsky & Rix 1997; Rudnick & Rix 1998). There are multiple ways in which one can quantify asymmetry, but here we choose to follow what was done for local spirals by Rix & Zaritsky (1995). This measurement is based on the azimuthal Fourier decomposition of the surface brightness along elliptical isophotes.

For the two most disk-like of the E+As (EA3 and 4), we calculate the Fourier decomposition of the F702W band surface brightness distribution. We use a grid with 24 azimuthal and 36 radial bins from semi-major axes of 4 to 200 pixels. The center of the azimuthal grid is identified as the brightest central point in the galaxy image. Figure 5 shows the amplitudes of the various first Fourier terms as a function of radius. In field spirals, $A_1 > 0.2$ is identified as strong lopsidedness, found in $\sim 20\%$ of the cases, and interpreted as the result of a recent interaction (other explanations, such as halo-induced disk sloshing have since been suggested; e.g., Levine & Sparke 1998; Kornreich et al 2002). EA3 has $A_1 \ll 0.2$ at all radii except in the transition region between the inner spiral arms and the tidal tails at $\sim 3-6$ kpc and at large radii where the uncertainties are large. Although EA4 has large A_1 within 3 kpc, which is consistent with the appearance of the residual image (Figure 2), $A_1 < 0.2$ for $1.5 < r_d < 2.5$, the range used in the study of field spirals. The

lopsidedness of EA3 and EA4 is consistent with that of normal spiral galaxies despite the cataclysmic event that occurred $\sim$ Gyr ago indicated by the spectra. This result has two possible interpretations: either these galaxies have had sufficient time to relax and "smooth out" interaction-induced asymmetries (e.g., Mihos 1995), or they are the result of encounters not strong enough to cause major dynamical damage. Of course, the latter possibility runs into the problem of how to trigger such a massive starburst without dynamically disturbing the galaxy.

3.4.   Color Gradients

The color gradients of E+As are constraints on merger models and clues as to what these galaxies will ultimately become. In Figure 6, we show the F702W−F439W color profiles of EA2-5, which are obtained by using the results from the ELLIPSE task and include the A-type K-correction. Because of the shallow exposure in F439W band, the color profiles are limited to $r \lesssim 2 - 3$ kpc, which is only 25% of the radial coverage available in the red. To derive the color profiles within the most central region ($< 0.5''$), we use the deconvolved images. However, because deconvolution can produce large artificial fluctuations in low signal-to-noise data, we cannot use the deconvolved F439W profiles in the outer regions of the galaxy. We compromise by using the deconvolved images for $r < 0.5''$ and the non-deconvolved images for $r > 0.5''$.

The overall colors of E+As are relatively blue globally due to the recent star formation (bottom panel of Figure 6). The radial extent of the blue colors confirms previous observations (Franx 1993; Caldwell et al. 1996; Norton et al. 2001) that the recent star formation region is not confined within the innermost regions. However, the color gradients, especially within 1 kpc of the centers, are as diverse as the overall morphologies. While, EA3 and EA5 have blue nuclei and become redder going outward, EA2 becomes bluer with radius, and EA4 shows a relatively flat profile.

The colors are the result of the complicated interplay between age, metallicity and dust. The lack of HI in these systems (Chang et al. 2001; Miller & Owen 2001) and of any patchiness in the images of EA2-5 argue against high levels of dust (but it is still possible that high density pockets of dust are present, particularly toward the nucleus of some of these systems). With the exception of EA1, none of the E+As show the irregular, filamentary structures expected from strong dust lanes. We thus conclude that the variety of color gradients within the inner few hundred parsecs reflects variations of the spatial distribution of the young population, which in some systems appears to be preferentially located near the center of the galaxy and in others appears to avoid the center. Perhaps this reflects differences in the types of encounter involved and its ability to drive true nuclear starbursts — e.g., differences between prograde and retrograde encounters (Barnes & Hernquist 1996), major versus minor mergers (Hernquist & Mihos 1995), or differences in the structural properties of the progenitor galaxies (Mihos & Hernquist 1996).

3.5.   Relationship to Fundamental Plane

To investigate whether E+As can evolve into E/S0 galaxies, we compare the stellar kinematics and structural parameters of E+As with "normal" early type galaxies. Norton et al. (2001) found that the old component of E+A galaxies is offset (brighter by ~ 0.6 mag) from the the local Faber-Jackson relation. Using the structural parameters that can only be measured using *HST* imaging, we extend this comparison to various projections of the Fundamental Plane (hereafter FP) in Figure 7. To compare our results with the FP of Jorgensen et al. (1996), we correct these observables to our adopted cosmology ($H_0 = 70$ km s^{-1} Mpc^{-1},

$(\Omega_M, \Omega_\Lambda) = (0.3, 0.7))$. Changes in the cosmological parameters only affect zero points in the FP equation. We use velocity dispersions from Norton et al. (2001) for the K-star component and the structural parameters from a single $r^{1/4}$ model [3]. We transform the F702W magnitude to a Gunn r magnitude using the average (F702W − Gunn r) color for galaxies of various Hubble type (Fukugita et al. 1995). The average $(r−\text{F702W})$ colors range from 0.56 for elliptical to 0.51 for Scd galaxies. Even for the extreme case of irregular (Im) galaxies, $(r − \text{F702W})$ is different by only ~ 0.1 magnitude from the average value of 0.54.

We show various projections of the FP in Figure 7. Figure 7(a) shows the face-on view of the FP given by $x = (2.21\ log\ r_e − 0.82\ log\langle I\rangle_e + 1.24\ log\ \sigma)/2.66$, $y = (1.24\ log\langle I\rangle_e + 0.82\ log\ \sigma)/1.49$ (see Jorgensen et al. (1996)). The dashed line indicates the bound set by the limiting magnitude, but the upper dotted boundary is not caused by a selection effect. Figure 7(b) shows the edge-on view of the FP along the long axis of the distribution, given by $y = 1.24\ log\ \sigma − 0.82\ log\langle I\rangle_e$. Figure 7(c) shows the Faber-Jackson relation. Figure 7(d) shows the correlations between r_e and $\langle \mu_e \rangle$.

The four E+As stand apart from the E/S0s in the edge-on view of the FP, but otherwise populate the same general region of the 3-D volume. The most striking deviation of the E+As among the scaling laws lies in the $\mu_e − r_e$ correlation. EA2-5 are more than a half magnitude brighter than the median E/S0 galaxies with the same effective radii. Especially, EA3 and EA4 have a large excess surface brightness over the dotted boundary of E/S0 galaxies in the FP. We measure the excess brightness to be 0.86 and 0.54 mag relative to the dotted upper boundary of the $\mu_e − r_e$ projection for EA3 and 4, respectively. As seen Figure 7(c), although EA2-5 have intermediate luminosities $(−22 < M_r < −20)$ in comparison to E and S0 galaxies, they have a large mean surface brightness within the effective radius.

Will E+As fade onto the locus of E/S0's after a few Gyr? We estimate the amount of fading within an effective radius using STARBURST99 models (Leitherer et al. 1999). Assuming solar metallicity, a Salpeter IMF, an underlying 5 Gyr-old population (not evolving), and a single instantaneous starburst with a mass fraction of 50%, the E+As will fade ~ 0.5 magnitudes during the first Gyr after the burst. This degree of fading places EA2, EA4, and EA5 on the E/S0 locus, but not EA3. This model is oversimplified, however. The evolutionary tracks in the $\mu_e − r_e$ projection will proceed from upper-left to lower-right, because of the decline of the mean surface brightness within r_e both due to fading and the inclusion of the larger fraction of the galaxy. But, calculating these effects requires a detailed knowledge of the spatial distribution of the young and old populations.

3.6.   Comparison with to "Core" and "Power-law" Ellipticals

Does the consistency in global surface brightness profiles between E+As and normal early-type galaxies (as discussed in §3.5) extend to the innermost radii? The recently discovered dichotomy in the central surface brightness profiles ("core" vs. "power-law"; Lauer et al. 1995; Faber et al. 1997) of normal early-type provides a framework for this comparison. In Figure 8, we plot the F702W surface brightness profiles for our E+As and the F555W profiles of Faber et al. (1997) sample (assuming $V − R = 0.5$ and adjusting for differences in adopted cosmology). The apparent lack of any central "break" and associated transition to a shallow cusp in the E+A profiles leads us to classify the E+As as "power-law" galaxies. Not only are the

---

[3]There is an issue as to which structural parameters (for the entire galaxy or the bulge only) one should use to construct the FP for S0 or disk galaxies. However, we opt to use the (r_e, μ_e) from a single $r^{1/4}$ profile, because we are comparing with Jorgensen et al. (1996), who also used single de Vaucouleurs profiles for S0's.

profiles shapes consistent, but the total luminosities of these E+As lie within the range spanned by normal power-law early-types, and any fading will place them even more securely in that range.

Although the profile shapes and total luminosities of E+As are consistent with those of power-law early-types, Figure 8 shows that the E+A surface brightness are generally higher. EA2 is consistent with the highest surface brightness normal power-law galaxies, and the other three E+As have even higher surface brightness. If fading of the young stellar population does not significantly alter the profile shape, then these galaxies will retain their power-law profiles. While we cannot be certain that the profiles will remain unchanged, the current inner profiles and total luminosities are consistent with E+A evolution into normal power-law early-type galaxies.

3.7. Discovery of Young Star Clusters

A specific type of asymmetric small-scale feature is the compact sources most visible in the residual images. We identify a set of these sources using SExtractor (Bertin & Arnouts 1996) to analyze both the combined and residual images. Because we expect stellar clusters to be unresolved at these distances (one pixel corresponds to $\sim 65 - 95$ pc at $z = 0.07 - 0.12$), confusion between real sources and hot pixels or background fluctuations is a serious problem. After testing various detection criteria and comparing visually, we decided to consider an object real only if it has at least three adjacent pixels that are each at a flux level 3 times above the local background rms. To estimate the local background level, we use a background mesh size for SExtractor of $\sim 4 - 8$ pixels, depending on the image. The residual images are used to detect compact sources close to the galaxy center, where the rapidly varying galaxy light complicates detections in the original images.

Using these criteria, we detect 35, 9, 29, 10 and 1 point-like sources within the PC images of EA1-5, respectively. These objects may be foreground stars, background compact sources, giant HII regions, or star clusters. Unfortunately, due to the insensitivity of the F439W band, we are able to obtain colors for only a few of the objects. The lack of emission lines in the spectra of these E+A galaxies (Zabludoff et al. 1996; Norton et al. 2001) suggests that these galaxies are not littered with giant HII regions. The spatial distribution of the compact objects suggests that the majority of these sources are associated with the E+As. For example, in EA1 almost all of the point sources are located around EA1 and its companion, and three of them lie in the bridge-like structure connecting the two galaxies. In EA2, some objects lie in the elongated tidal tails. In EA3, five to six unresolved objects surround the nucleus of EA3 and form a concentric circle. We apply a Kolmogorov-Smirnoff (K-S) one-sample test to find the probability that the radial distributions of the compact sources are drawn from a random distribution. We show the cumulative distribution of the angular distances from the center of each galaxy in Figure 9. There is almost zero probability that the sources follow the random distribution, indicating that the detected compact sources are truly associated with the E+A galaxies. Because of the post-starburst nature of E+A galaxies and the discovery of numerous young clusters in ongoing mergers (e.g., Holtzman et al. 1992; Whitmore et al. 1993), it is likely that the majority of these objects are relatively young star clusters.

Like the morphological diversity of the E+As themselves, the number of cluster candidates varies widely among EA1-5. In particular, the difference between EA3 and EA5 is remarkable because these otherwise appear to have comparable masses (the velocity dispersions of their old populations are the same and the luminosity ratio is ~ 0.5). The principal difference between these systems is that EA5 is more distant. To determine whether the distance difference is responsible for the difference in detected sources, we model the

detectability of the point sources as a function of distance. For a given size (half-light radius) and brightness, we generate two dimensional surface brightness distributions of the model clusters for a King profile (King 1966) with concentration $c = 0.5 - 2.5$. We convolve the model profiles with the PC PSF generated from the TinyTim software (Krist & Hook 1999). All models and PSFs are constructed at a resolution of 1/10th of a PC pixel, re-binned to the original image size, and smeared using the pixel smearing kernel. After adding the Poisson noise and sky background, we attempt to detect the cluster using the same detection criteria that we apply to the original images. The position on the PC and the spectral variation of the PSF do not affect our detection threshold.

The number of detected pixels above 3σ is nearly insensitive to the size of the sources and the shape of the profile in the subpixel regime. In other words, the images of point sources give us little or no information about their spatial structures, but they can be detected if they are sufficiently bright. We adopt the detection limit as the magnitude at which the number of detected pixels above 3σ drops below three pixels. The number of compact sources above EA5's detection limit ($M_R < -12.5 \pm 0.25$) and well outside the E+A are 6 to 16 for EA3 and is 1 for EA5. The uncertainty in the detection limit arises from uncertainties in the aperture correction and photometry. Assuming EA5 has the same number of the compact sources as EA3, we would expect to detect 3 to 8 sources in EA5 after rough scaling of the projected area occupied by the detections around each galaxy. The statistics of our sample thus preclude us from distinguishing between the cluster populations of EA3 and EA5. If the difference is significant, it might reflect a difference in the starburst (strength or progenitors) or an age difference. The latter possibility is consistent with the observation that EA5 has the reddest D_{4000} and is the most symmetric among our sample.

Matching the observed colors of the cluster candidates with the predictions of stellar population synthesis models can help break the degeneracy between the age and starburst strength of our post-merger E+As. We show the evolution of the color and brightness of a simple stellar population based on Starburst99 models (Leitherer et al. 1999) in Figure 10. Because of the unknown SEDs of our sources, the K correction of the observed colors is problematic. To avoid applying an uncertain K correction, we calculate the redshifted (F439W-F702W) colors from the model spectra provided from Starburst99. Superposed on the various models, we show the range of the colors observed and the corresponding range of ages for each of the five point-like sources in EA1 with $\sigma(\mathrm{F439W} - \mathrm{F702W}) < 0.25$ and sufficient S/N. They are identified by eye in the F439W band and are not located in the crowded region. Because the absence of the O, B stellar signatures (Zabludoff et al. 1996; Norton et al. 2001) suggest that the ages of the clusters are older than 10^7 yr, we rule out the solutions in the double trough of the model. Assuming a Salpeter IMF that extends from 1 to 100 $M_\odot$, solar metallicity ($Z = 0.020$), and an instantaneous starburst, we estimate the ages of the candidate clusters to be between ~ 30 Myr and 500 Myr.

We applied the following statistical test to constrain the time since the starburst under the assumption that all the candidate clusters formed at the same time and have a spread of estimated age due to photometric errors. For each model age, we draw a thousand samples of five clusters each with colors scattered according to a Gaussian of dispersion 0.2 mag. We calculate the percentage of simulations that have a median color as far from the true color as the observed median color. If that number is 5% or less, the model is rejected. Because of the slow evolution of colors in the relevant age range, we can constrain the age of clusters (time elapsed since the starburst) to only $\sim 35 - 450$ Myr at the 95% confidence level (see the horizontal line in Figure 10). While our constraint on the age is drawn from only a few cluster candidates, this range is as good as the typical age ranges that Leonardi & Rose (1996) derived using CaII and $H\delta/\lambda4045$ indices from the integrated spectra of E+A galaxies. Because any reddening by the host galaxy will make the sources look older, our estimated ages are upper limits on the true ages. However, it is unlikely that the reddening

affects our results seriously because the five sources are at large radii, where the extinction should be minor compared to the galaxy center. To improve upon the age estimate, in particular to reduce contamination, to correct the reddening, and to get more precise ages for the sources, ideally we would need deep multicolor photometry to produce a two-color diagram like Fig. 6 in Harris et al. (2001). However, we can see from the present analysis that we would benefit from just more clusters with colors. We conclude that the derived ages are consistent with what we expect on the basis of the integrated galaxy spectra, again supporting the claim that these are stellar clusters associated with the E+A phenomenon, and suggesting that this is part of a population of clusters formed during the E+A phase.

We compare the R band cluster luminosities of EA1, EA3, the Milky Way globular clusters (Harris 1996) and the clusters in starbursting, merging systems (e.g., NGC3597, Carlson et al 1999). If the compact sources in the E+As are clusters, they are much brighter ($M_R \sim -13$) than Galactic globular clusters ($M_R > -11$) and similar to clusters in galaxies with on-going starburst. The latter agreement supports the interpretation that we have identified the bright end of a population (e.g., $M_R \sim -14$ in NGC3597) of star clusters formed during a starburst that occurred < 1 Gyr ago. A fading of several magnitudes is required for these systems to resemble the massive end of the Milky Way cluster population.

3.8. Implications for High Redshift Interacting Galaxies

The difficulty we have experienced in determining whether these E+As have a disk component, have tidal components, and are asymmetric suggests that at high redshift these galaxies might be classified as "normal" morphologically. For example, the tidal tails that connect onto what may be a disk would naturally be interpreted as spiral arms if one is not able to trace the tails out to large radii. To better understand this effect, we rebin the F702W band image of EA3 and fade it artificially according to our adopted cosmology to mimic its appearance at higher redshift (Figure 11). The rebined images are convolved with the PSF, and the sky background and noise proportional to the exposure time are added to the redshifted images. For each image, we assume the same exposure time (2100s) and average sky brightness. The tidal features are lost at a redshift over ~ 0.5 (see also Mihos 1995; Hibbard & Vacca 1997), and EA3 appears to be a normal spiral or S0 galaxy. The mean surface brightness of the tidal tails of EA3 is $\sim 24 - 25$ mag arcsec^{-2}. This exercise suggests that some of the disky E+A galaxies found frequently in distant clusters might be misclassified as non-interacting disk galaxies and nevertheless have tidal features like EA2-4. The lack of apparent tidal features and of asymmetry at high redshift should not be interpreted directly as an absence of interactions.

4. Summary

Using *HST* imaging, we have obtained high resolution images of five E+Ai galaxies. Our results, when coupled with studies of E+A kinematics, star formation histories, and gas content, argue that E+As are in transition between late and early types, a missing link in the evolution of galaxies. Our principal findings are:

1. Four (EA1-4) of the five E+As are morphologically disturbed (with tidal tails and shell-like structures), consistent with being relics of galaxy-galaxy interactions. The dramatic tidal features found in EA1, 2, and 3 further confirm that galaxy-galaxy mergers are at least one mechanism that triggers the starburst that leads to the E+A phase.

2. E+As have diverse morphologies. Even in this small sample, one highly disturbed galaxy cannot be morphologically classified (EA1) and one regular galaxy could plausibly be classified as a barred S0 galaxy (EA5). Two other galaxies (EA3 and 4) seem to contain disk components. The striking aspect of this morphological variety is that all of these galaxies have been selected on the basis of their very similar spectra.

3. The bulge fractions of these systems are consistent with elliptical and S0 galaxies. E+As have a central structure consistent with "normal" power-law early type galaxies (Faber et al. 1997), although at present the E+As have significantly higher surface brightnesses. This is the first direct confirmation that power-law elliptical galaxies can be formed from gas-rich mergers.

4. E+As are blue due to recent star formation, but their color gradients in the central region are as diverse as their morphologies. Two galaxies (EA3 and 5) have extremely blue cores that redden toward the outer regions, one (EA4) has a relatively flat profile, and one (EA2) has a redder core within a few kpc. The red core is particularly puzzling from the standpoint of merger models that predict gas inflow into the center and a subsequent starburst. It is possible that the red color arises from dust extinction, but we see no evidence for the filamentary structure usually associated with dust lanes.

5. E+As stand apart from the E/S0s in the Fundamental Plane mainly due to their high central surface brightness. Fading of the young stellar population and a corresponding increase in r_e (if the young population is more concentrated than the underlying population) will cause the systems to migrate toward the locus of E/S0s in time. Without a detailed knowledge of the distribution of young and old stars it is not possible to model this evolution precisely.

6. We find compact sources associated with E+A galaxies. Although some of these sources could be foreground stars, giant HII regions, or background objects, we conclude that the majority are star clusters that formed during the starburst phase, such as those found in nearby starburst galaxies. These systems are similar in luminosity to the brightest clusters in NGC 3597 (Carlson et al. 1999) and have ages consistent with that expected for the time elapsed since the starburst (several 10^8 yrs). They are much brighter ($M_R \sim -13$) than Galactic globular clusters, but will fade over a Hubble time to be consistent with the most massive Milky Way clusters. Further study of these systems might provide the elusive chronometer for lifting the age/burst-strength degeneracy for post-merger galaxies.

One valuable lesson of our work is that despite the recent interactions that at least some of these E+As have experienced, one of the standard tests for interactions (the lopsidedness measure based on the azimuthal Fourier decomposition of the isophotes) fails to identify these systems as having experienced a recent interaction. The tidal features are sufficiently faint and the inner surface brightness profiles sufficiently regular that the galaxies are measured to be symmetric. Such indicators should therefore be used with caution on large-scale surveys and at high-redshifts because they obviously miss at least some recently interacting systems. Furthermore, in a system that one does not suspect to be interacting, the tidal tails can easily be misidentified as spiral arms.

This work described the observations of the five bluest E+A galaxies in LCRS sample with HST/WFPC2. To confirm the various results presented here and determine whether this subset was biased by the color selection requires a study of the remainder of the LCRS sample. We are currently obtaining HST/ACS imaging of those galaxies.

REFERENCES

Ashman, K. M. & Zepf, S. E. 1992, ApJ, 384, 50

Barnes, J. E. 1988, ApJ, 331, 699

Barnes, J. E. & Hernquist, L. 1996, ApJ, 471, 115

Bendo, G. J. & Barnes, J. E. 2000, MNRAS, 316, 315

Bertin, E. & Arnouts, S. 1996, A&AS, 117, 393

Butcher, H. & Oemler, A. 1978, ApJ, 219, 18

Caldwell, N., Rose, J. A., Franx, M., & Leonardi, A. J. 1996, AJ, 111, 78

Carlson, M. N. et al. 1999, AJ, 117, 1700

Chang, T., van Gorkom, J. H., Zabludoff, A. I., Zaritsky, D., & Mihos, J. C. 2001, AJ, 121, 1965

Couch, W. J. & Sharples, R. M. 1987, MNRAS, 229, 423

Dressler, A. & Gunn, J. E. 1983, ApJ, 270, 7

Dressler, A., Smail, I., Poggianti, B. M., Butcher, H., Couch, W. J., Ellis, R. S., & Oemler, A. J. 1999, ApJS, 122, 51

Faber, S. M., Tremaine, S., Ajhar, E. A., Byun, Y., Dressler, A., Gebhardt, K., Grillmair, C., Kormendy, J., Lauer, T. R., & Richstone, D. 1997, AJ, 114, 1771

Franx, M. 1993, ApJ, 407, L5

Fukugita, M., Shimasaku, K., & Ichikawa, T. 1995, PASP, 107, 945

Graham, A. W. 2002, MNRAS, 334, 859

Graham, A. W., Erwin, P., Caon, N., & Trujillo, I. 2001, ApJ, 563, L11

Gunn, J. E. & Stryker, L. L. 1983, ApJS, 52, 121

Harris, J., Calzetti, D., Gallagher, J. S., Conselice, C. J., & Smith, D. A. 2001, AJ, 122, 3046

Harris, W. E. 1996, AJ, 112, 1487

Hernquist, L. & Mihos, J. C. 1995, ApJ, 448, 41

Hibbard, J. E. & Vacca, W. D. 1997, AJ, 114, 1741

Holtzman, J. A. et al. 1992, AJ, 103, 691

Holtzman, J. A., Burrows, C. J., Casertano, S., Hester, J. J., Trauger, J. T., Watson, A. M., & Worthey, G. 1995, PASP, 107, 1065

Jorgensen, I., Franx, M., & Kjaergaard, P. 1996, MNRAS, 280, 167

Kelson, D. D., Illingworth, G. D., van Dokkum, P. G., & Franx, M. 2000, ApJ, 531, 137

Kent, S. M. 1985, ApJS, 59, 115

King, I. R. 1966, AJ, 71, 64

Kornreich, D. A., Lovelace, R. V. E., & Haynes, M. P. 2002, ApJ, 580, 705

Krist, J. & Hook, R. 1999, The TinyTim User's Guide(Baltimore: STSCI)

Lauer, T. R., Ajhar, E. A., Byun, Y.-I., Dressler, A., Faber, S. M., Grillmair, C., Kormendy, J., Richstone, D., & Tremaine, S. 1995, AJ, 110, 2622

Lauer, T. R., Faber, S. M., Ajhar, E. A., Grillmair, C. J., & Scowen, P. A. 1998, AJ, 116, 2263

Leonardi, A. J. & Rose, J. A. 1996, AJ, 111, 182

Levine, S. E. & Sparke, L. S. 1998, ApJ, 496, L13

Lucy, L. B. 1974, AJ, 79, 745

Leitherer, C. et al. 1999, ApJS, 123, 3

Mihos, J. C. 1995, ApJ, 438, L75

Mihos, J. C. & Hernquist, L. 1994, ApJ, 431, L9

Mihos, J. C. & Hernquist, L. 1996, ApJ, 464, 641

Miller, N. A. & Owen, F. N. 2001, ApJ, 554, L25

Naab, T. 2000, Ph.D. thesis

Norton, S. A., Gebhardt, K., Zabludoff, A. I., & Zaritsky, D. 2001, ApJ, 557, 150

Nugent, P., Kim, A., & Perlmutter, S. 2002, PASP, 114, 803

Peng, C. Y., Ho, L. C., Impey, C. D., & Rix, H. 2002, AJ, 124, 266

Poggianti, B. M., Smail, I., Dressler, A., Couch, W. J., Barger, A. J., Butcher, H., Ellis, R. S., & Oemler, A. J. 1999, ApJ, 518, 576

Quintero, A. D. et al. 2003, submitted to ApJ, astro-ph/0307074

Richardson, W. H. 1972, J. Opt. Soc. A., 62, 5

Rix, H. & Zaritsky, D. 1995, ApJ, 447, 82

Rudnick, G. & Rix, H. 1998, AJ, 116, 1163

Salpeter, E. E. 1955, ApJ, 121, 161

Schlegel, D. J., Finkbeiner, D. P., & Davis, M. 1998, ApJ, 500, 525

Toomre, A. 1977, in "The Evolution of Galaxies and Stellar Populations", eds. B. Tinsley and R.B. Larson (New Haven: Yale Univ.), p. 401

Whitmore, B. C., Schweizer, F., Leitherer, C., Borne, K., & Robert, C. 1993, AJ, 106, 1354

Zabludoff, A. I., Zaritsky, D., Lin, H., Tucker, D., Hashimoto, Y., Shectman, S. A., Oemler, A., & Kirshner, R. P. 1996, ApJ, 466, 104

Zaritsky, D. & Rix, H. 1997, ApJ, 477, 118

Table 1.   Properties of galaxies

ID	R.A. (1950.0)	Dec. (1950.0)	z	$kpc/''$	f_A [a]	$\langle V_{rot}\rangle$ [a]		σ (kms^{-1}) [a]		cluster ?
						Old	Young	Old	Young	
EA1	10 58 48.97	-11 54 9.80	0.0746	1.417	0.80	24^{+57}_{-54}	19^{+17}_{-17}	35^{+39}_{-35}	23^{+53}_{-23}	N
EA2	2 15 43.24	-44 46 36.70	0.0987	1.823	0.42	23^{+16}_{-20}	22^{+24}_{-25}	202^{+17}_{-16}	193^{+32}_{-46}	N
EA3	12 6 31.34	-12 5 55.40	0.0810	1.527	0.59	23^{+17}_{-23}	25^{+18}_{-17}	120^{+22}_{-20}	56^{+35}_{-32}	N
EA4	3 58 23.42	-44 43 40.29	0.1012	1.864	0.56	1^{+8}_{-9}	35^{+15}_{-16}	131^{+9}_{-9}	246^{+24}_{-25}	Y
EA5	1 56 0.12	-44 51 49.00	0.1172	2.119	0.42	33^{+24}_{-25}	52^{+34}_{-18}	120^{+7}_{-8}	94^{+34}_{-41}	N

[a]Data from Norton et al. (2001)

Table 2.   Magnitudes and colors of E+A galaxies

	F439W		F702W		F439W$-$F702W
ID	$m\ (< 4.5'')$	M	$m\ (< 4.5'')$	M	$(r < r_e)$
EA1	17.95 $\pm$ 0.02	-19.97	17.18 $\pm$ 0.01	-20.40	—
EA2	18.09 $\pm$ 0.02	-20.50	16.44 $\pm$ 0.01	-21.70	1.10 $\pm$ 0.01
EA3	16.75 $\pm$ 0.01	-21.52	15.34 $\pm$ 0.01	-22.49	0.80 $\pm$ 0.01
EA4	17.47 $\pm$ 0.01	-21.17	15.86 $\pm$ 0.01	-22.31	1.18 $\pm$ 0.01
EA5	18.58 $\pm$ 0.04	-20.51	16.83 $\pm$ 0.01	-21.67	0.99 $\pm$ 0.01

Table 3.   K corrections for A dwarf and K giant

		A dwarf		K giant	
ID	z	K(F439W)	K(F702W)	K(F439W)	K(F702W)
EA1	0.0746	0.136 $\pm$0.035	-0.148 $\pm$0.022	0.755 $\pm$0.123	0.042 $\pm$0.032
EA2	0.0987	0.233 $\pm$0.038	-0.192 $\pm$0.028	0.991 $\pm$0.168	0.065 $\pm$0.038
EA3	0.0810	0.157 $\pm$0.036	-0.160 $\pm$0.024	0.823 $\pm$0.136	0.048 $\pm$0.034
EA4	0.1012	0.246 $\pm$0.039	-0.196 $\pm$0.029	1.016 $\pm$0.172	0.068 $\pm$0.039
EA5	0.1172	0.340 $\pm$0.042	-0.225 $\pm$0.033	1.176 $\pm$0.192	0.084 $\pm$0.043

Table 4.   Structural parameters

	$r^{1/4}$-Law			Sérsic $r^{1/n}$-Law			
ID	r_e (kpc)	μ_e	χ^2_ν	r_e (kpc)	μ_e	n	χ^2_ν
EA2	2.74 $\pm$ 0.14	19.99 $\pm$ 0.09	1.72	4.49 $\pm$ 0.98	21.10 $\pm$ 0.39	6.22 $\pm$ 0.53	1.62
EA3	1.79 $\pm$ 0.07	18.56 $\pm$ 0.07	2.08	3.74 $\pm$ 0.64	20.19 $\pm$ 0.28	8.73 $\pm$ 0.45	1.51
EA4	2.07 $\pm$ 0.07	19.22 $\pm$ 0.06	1.61	2.43 $\pm$ 0.24	19.61 $\pm$ 0.17	5.10 $\pm$ 0.25	1.56
EA5	1.62 $\pm$ 0.06	18.85 $\pm$ 0.07	1.49	2.39 $\pm$ 0.38	19.70 $\pm$ 0.31	6.40 $\pm$ 0.56	1.45

Table 5.   Bulge-disk decompositions

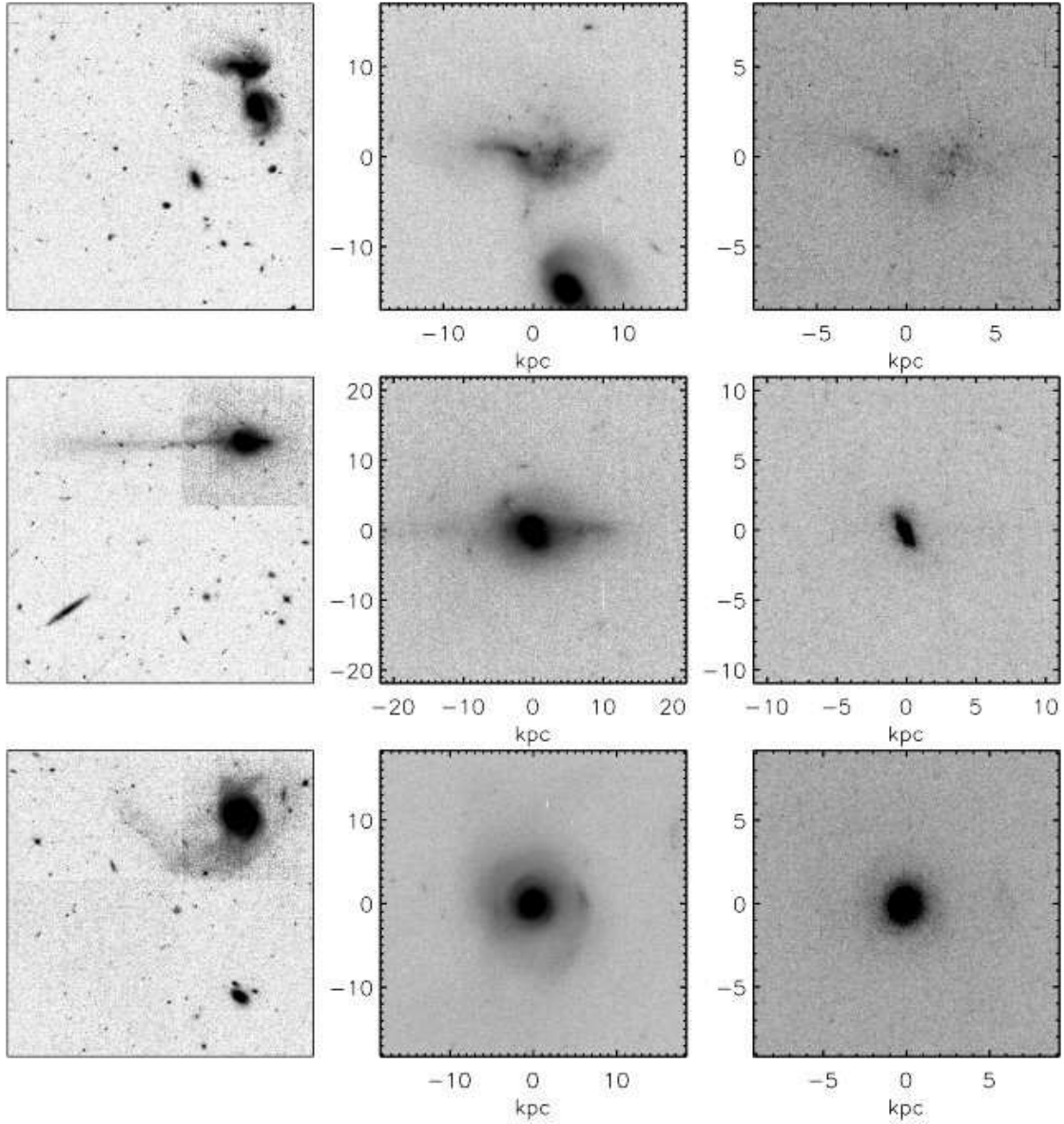| ID	Bulge		Disk		χ^2_ν	B/T
	r_e (kpc)	μ_e	r_d (kpc)	μ_d		
EA3	0.69 ± 0.03	17.02 ± 0.05	3.57 ± 0.22	19.30 ± 0.14	1.58	0.56
EA4	1.11 ± 0.05	18.11 ± 0.05	3.44 ± 0.16	19.50 ± 0.12	1.48	0.62
EA5	1.14 ± 0.03	18.23 ± 0.04	4.01 ± 0.45	21.00 ± 0.21	1.45	0.70

Fig. 1.— *HST* WFPC2 images of five E+A galaxies. From top to bottom, EA1 to EA5. (*left column*) WFPC2 mosaic images in high contrast. Notice the dramatic tidal tails. (*middle column*) High resolution F702W band PC images in low contrast. (*right column*) Central regions in F439W band. The size of each field is $\sim 80''$, $24''$, and $12''$ (left to right), and the pixel scale in the middle and right columns is $0''.046$/pixel.
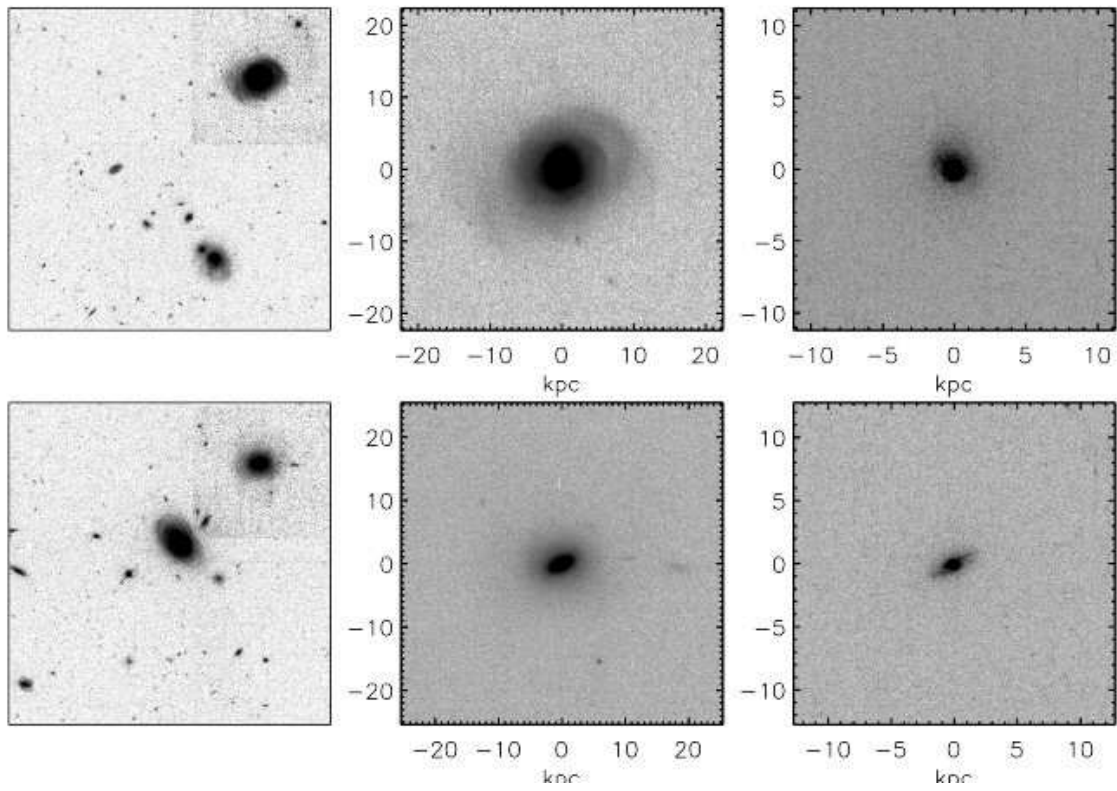
Fig. 1.— Continued.
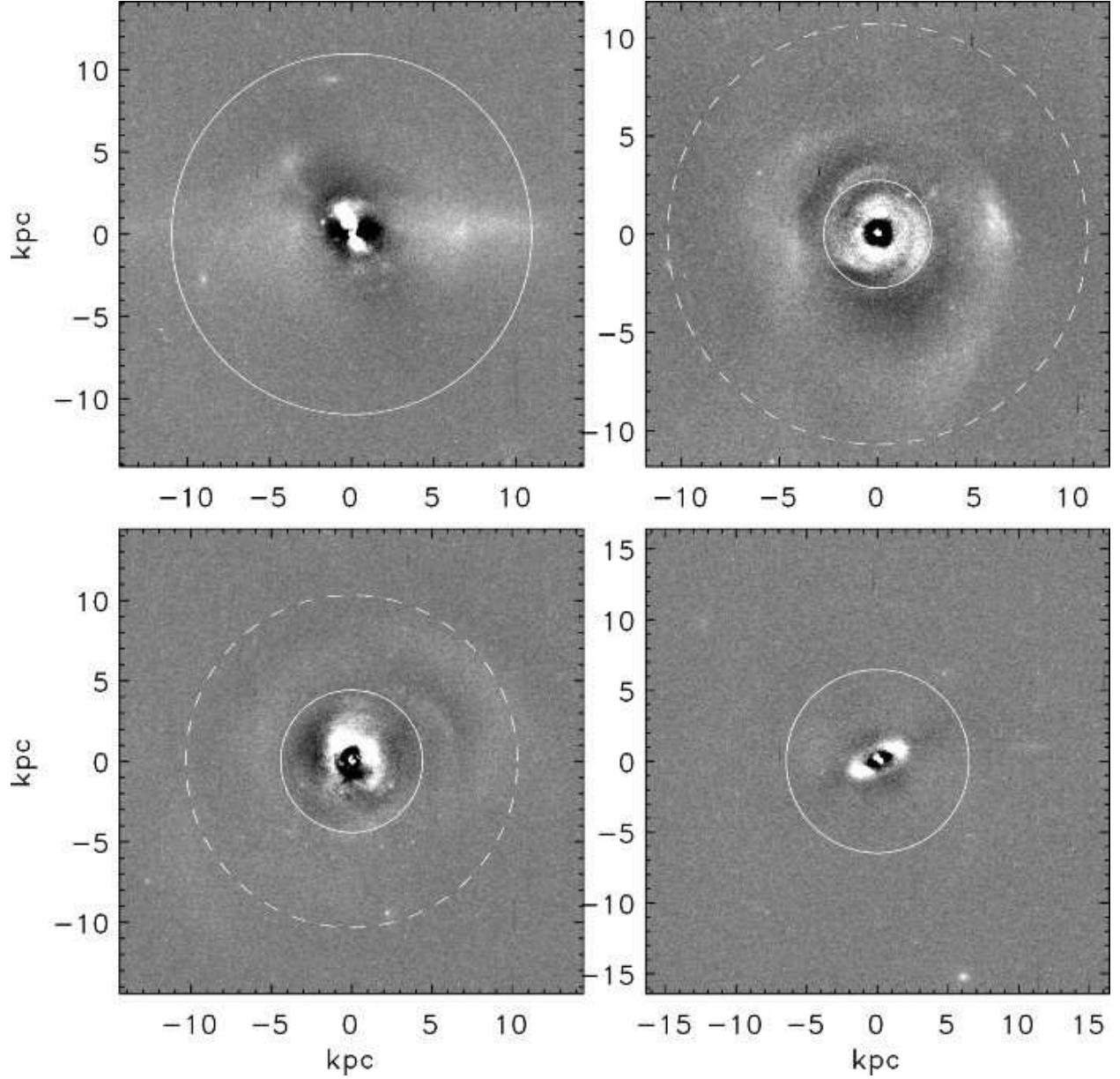
Fig. 2.— Residual images ($15.5'' \times 15.5''$) obtained by subtracting the smooth and symmetric model images from the data. EA3 and EA4 : $r^{1/4}$ bulge + exponential disk model. EA2 and EA5 : $r^{1/4}$ bulge only. The solid and dashed circles represent $4r_e$ and $3r_d$ (if bulge+disk decomposition was done), respectively. The relative asymmetric light — excess (deficit) — within a $10''$ radius is 16(8)%, 6(5)%, 8(9)% and 9(8)% of the symmetric model components for EA2-5, respectively.
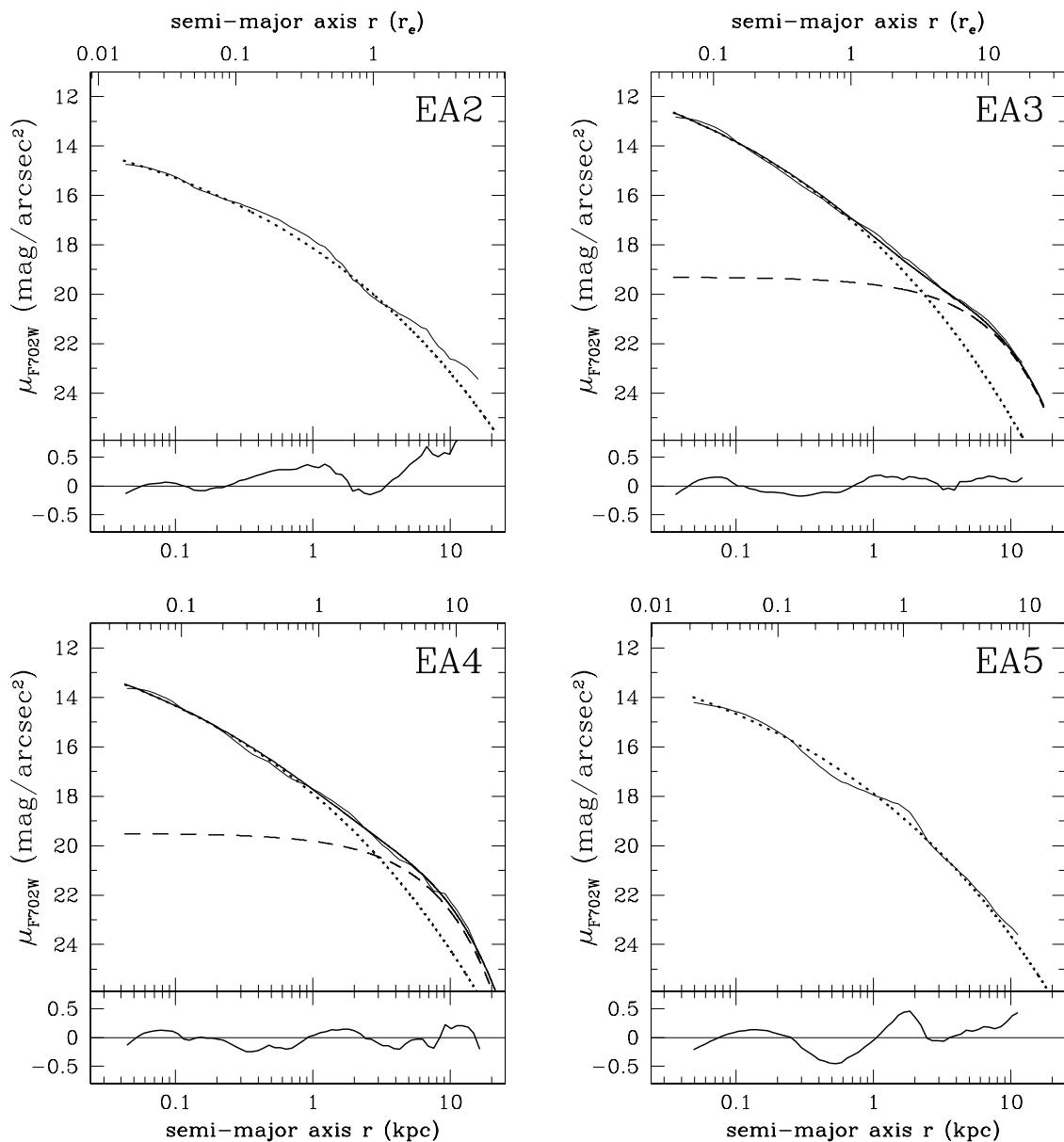
Fig. 3.— F702W radial surface brightness profiles. The thin solid lines show the radial profiles obtained from ELLIPSE, the dotted lines show the bulge components fitted to the $r^{1/4}$ law, and the dashed lines show the disk/tidal components fitted to the exponential law. The thick solid lines are the superposition of the bulge and disk components. Pure bulge + disk decomposition was done only for EA3 and EA4 (fitting EA5 was more complicated, see text and Figure 4). The top axis of each panel is the effective radius r_e of the bulge component of each galaxy. Bottom panels show the difference between the data (ELLIPSE) and fits (GALFIT).
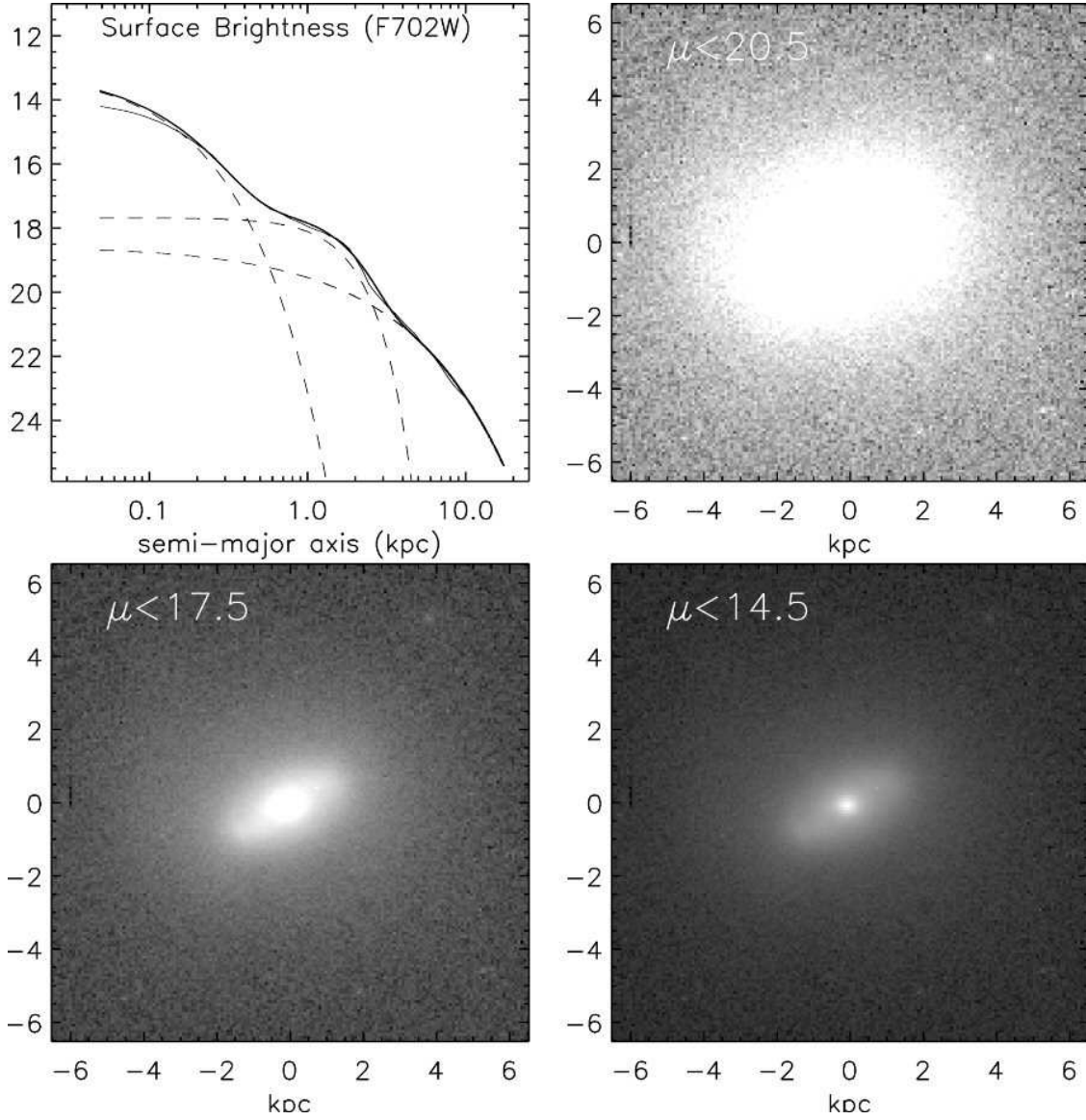
Fig. 4.— EA5 galaxy in different contrasts. EA5 shows three components — an extended light distribution in the outer part, a bar structure, and a very bright blue central nucleus. (*Upper left panel*) Three-component decomposition of EA5. The dashed lines represent each component. Solid thin and thick lines show the data and the sum of the three model components ($n = 1.1$, 0.5, and 1.5 from inside to outside), respectively.
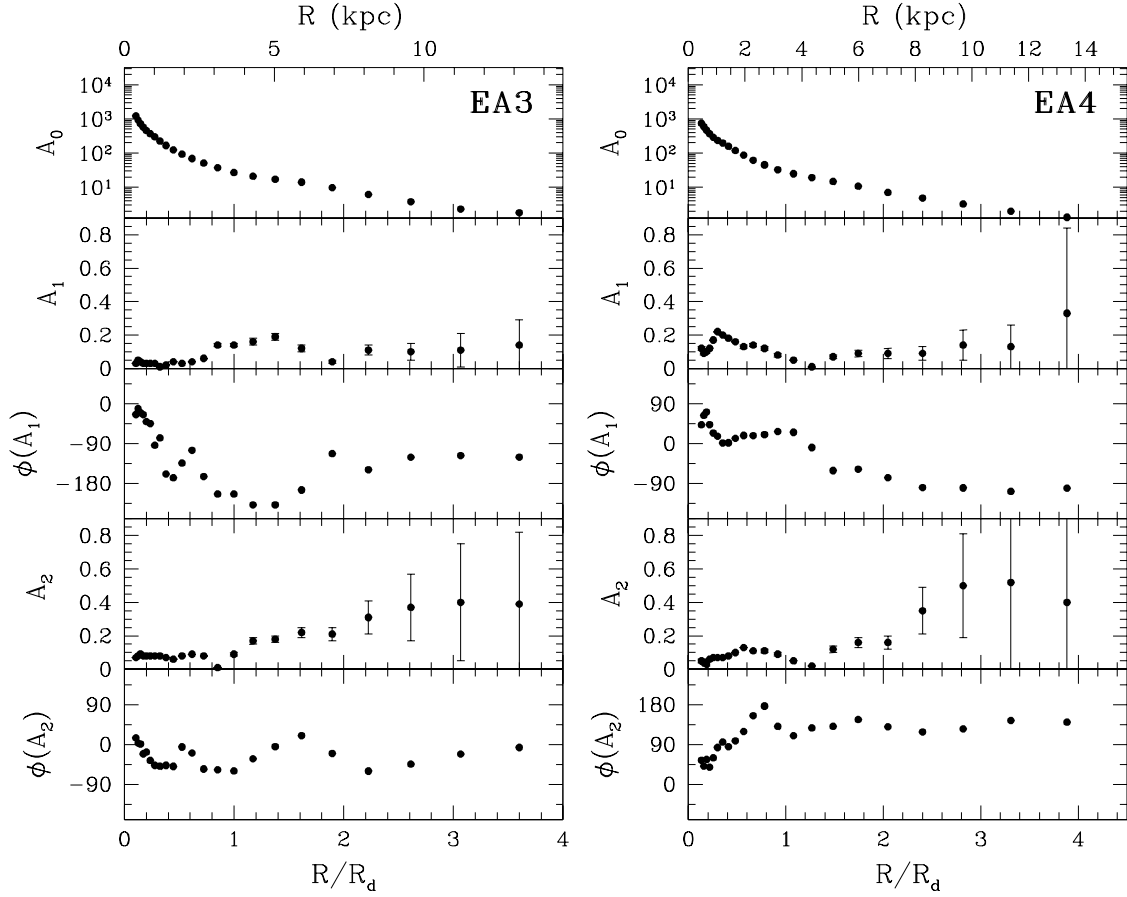
Fig. 5.— Amplitudes and phases of each Fourier component in the F702W images. Radius is plotted in disk scale units and kpc. A_m and $\phi(A_m)$ are the m-th order Fourier amplitudes and phase angles, respectively. The zeroth order component A_0 has no phase and reflects the mean flux at the given radius. The first order component A_1 denotes the lopsidedness of the galaxy at the given radius.
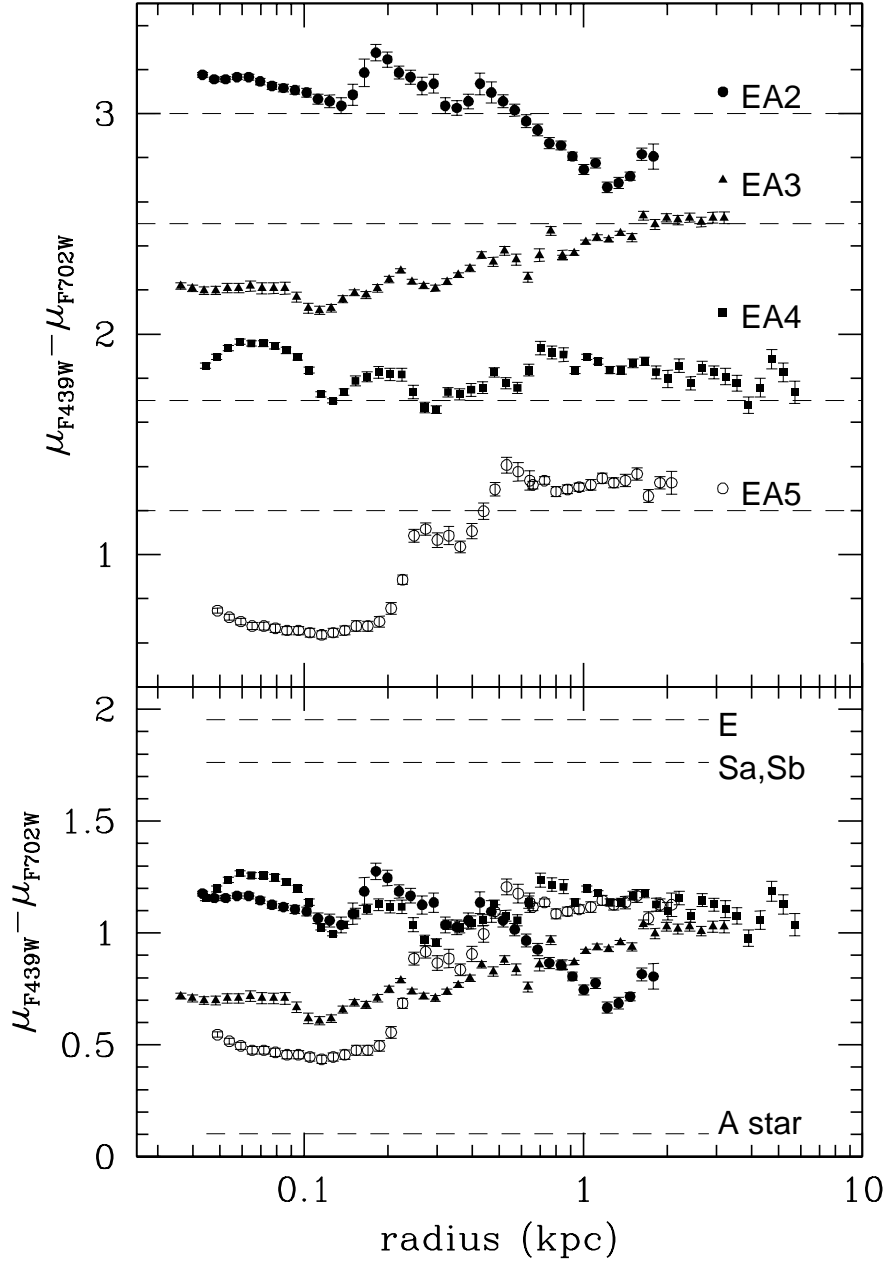
Fig. 6.— (F702W − F439W) color profiles of four E+A galaxies. The zero point in the color axis is arbitrary in the upper panel. The dashed (F702W − F439W) = 1.0 lines for each color profile are shown for reference. The dashed lines in the lower panel represent the typical colors of elliptical galaxies, spiral galaxies, and A stars. Notice the diversity of the color gradients within 1 kpc, which is reminiscent of their morphological diversity.
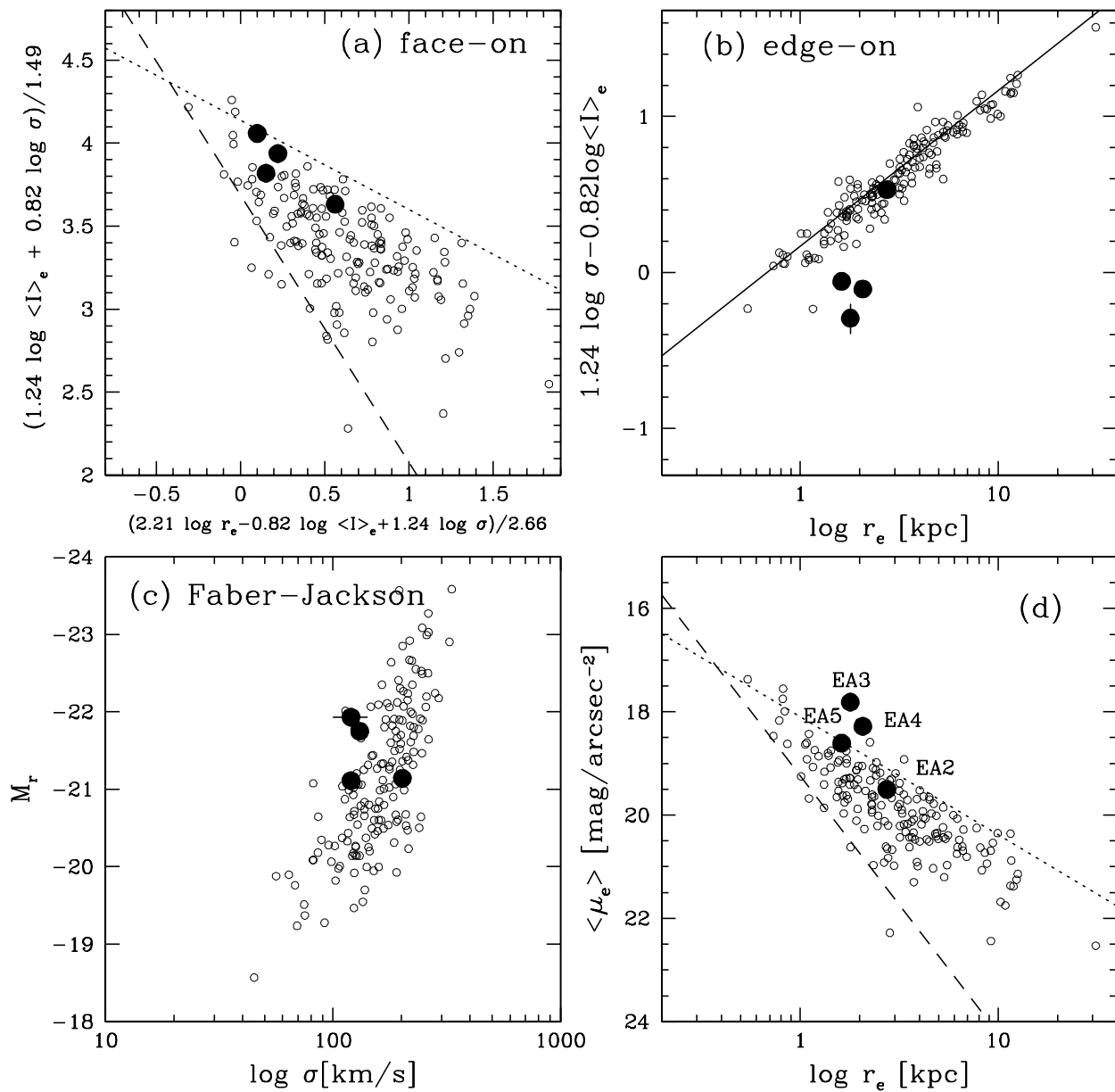
Fig. 7.— Relative position of four E+A galaxies in the Fundamental Plane (FP). The small open circles are data from Jorgensen et al (1996). (a) Face-on view of the FP as in Jorgensen et al (1996). The dashed line indicates the boundary set by the limiting magnitude, but the upper dotted line is not caused by a selection effect. (b) Edge-on view of the FP in the longest direction (dashed line in panel (a)) of distribution. (c) The Faber-Jackson relation. Our galaxies occupy a small region in the parameter space. (d) The $r_e - \mu_e$ correlations of early type galaxies and the four E+As. Notice the deviation of EA3 and EA4 from the average relation ($\sim 0.5 - 1.0$ magnitudes brighter than E/S0 galaxies within one effective radius).
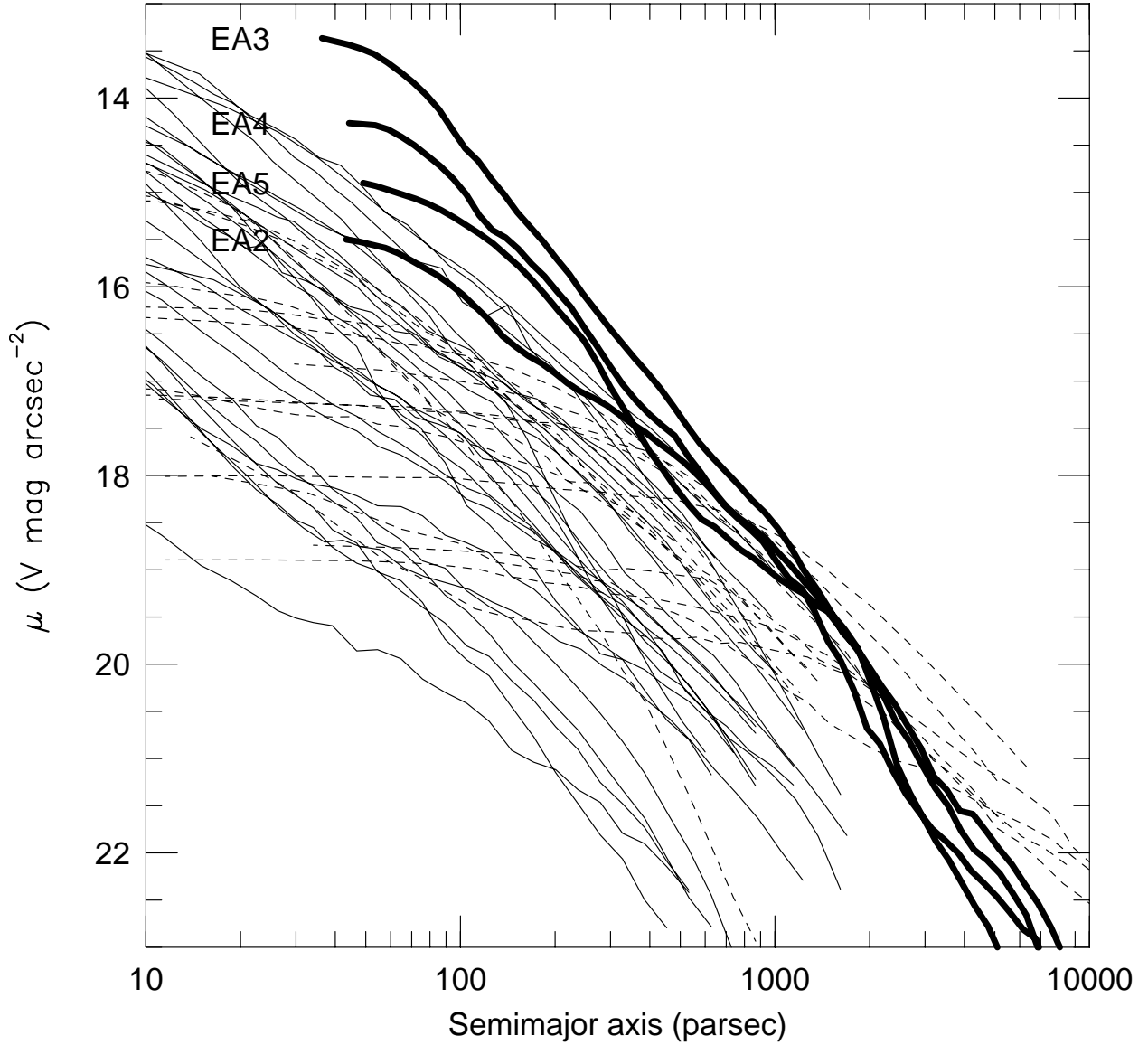
Fig. 8.— The F702W surface brightness plots of the sample E+A galaxies versus those of normal early-type galaxies (Faber et al. 1997). (The present figure is an adaptation of Faber et al.'s Figure 1.) The E+As are matched to the Faber et al. (1997) scale by assuming $V - R = 0.5$ mag and adopting $H_0 = 70$. Power-law galaxies are plotted as solid lines; core galaxies are plotted as dashed lines. E+A galaxies (thick solid lines) have profiles like those of normal power-law early-type galaxies, but scaled-up in surface brightness.
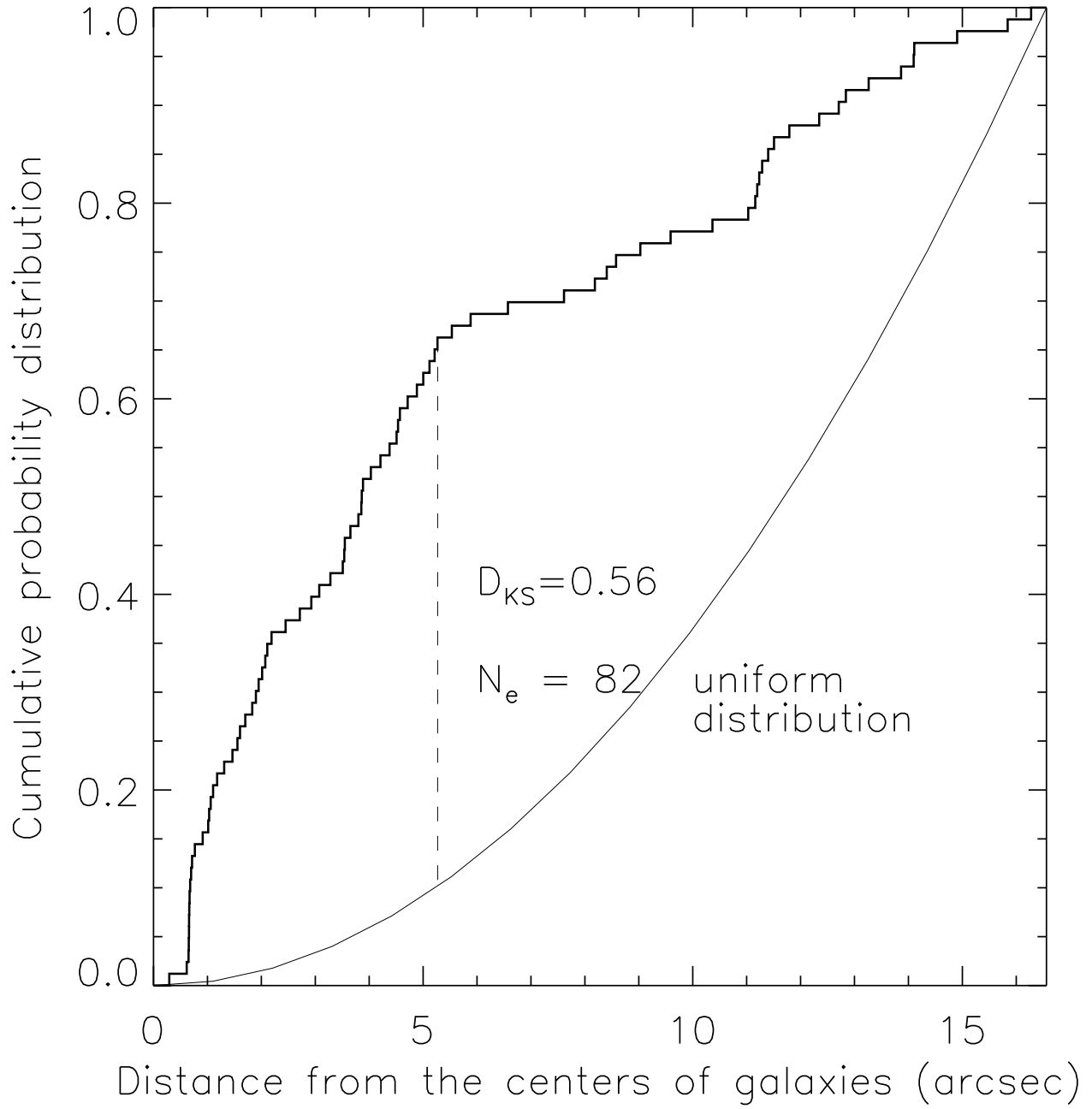
Fig. 9.— Cumulative distribution of the angular distances of the candidate clusters from the center of the E+As. Thin solid line represents a uniform (or random) distribution, $P(< r) \propto r^2$.
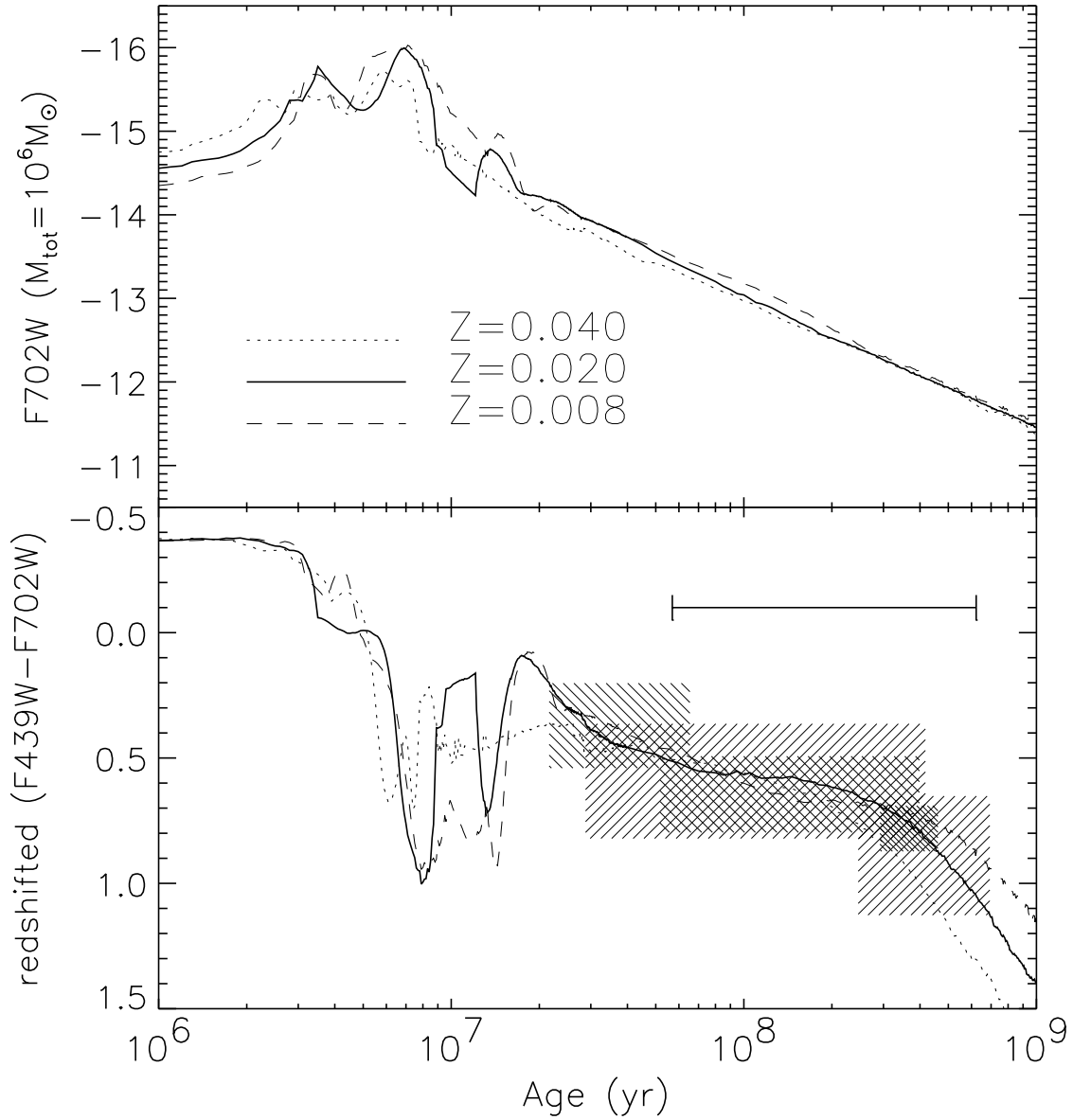
Fig. 10.— The evolution of the redshifted (F439W-F702W) color and F702W magnitude of a simple stellar population calculated from the models of Starburst99 (Leitherer et al. 1999). Evolution is shown for a single starburst, Salpeter initial mass function (Salpeter 1955), and three different metallicities. The shaded regions represent the range of colors observed and the corresponding range of ages for each cluster candidate in EA1. These candidates are identified in both the F702W and F439W image. The horizontal line in the bottom panel indicates the 95% confidence level of the estimated single age of the clusters — the time elapsed since the starburst.
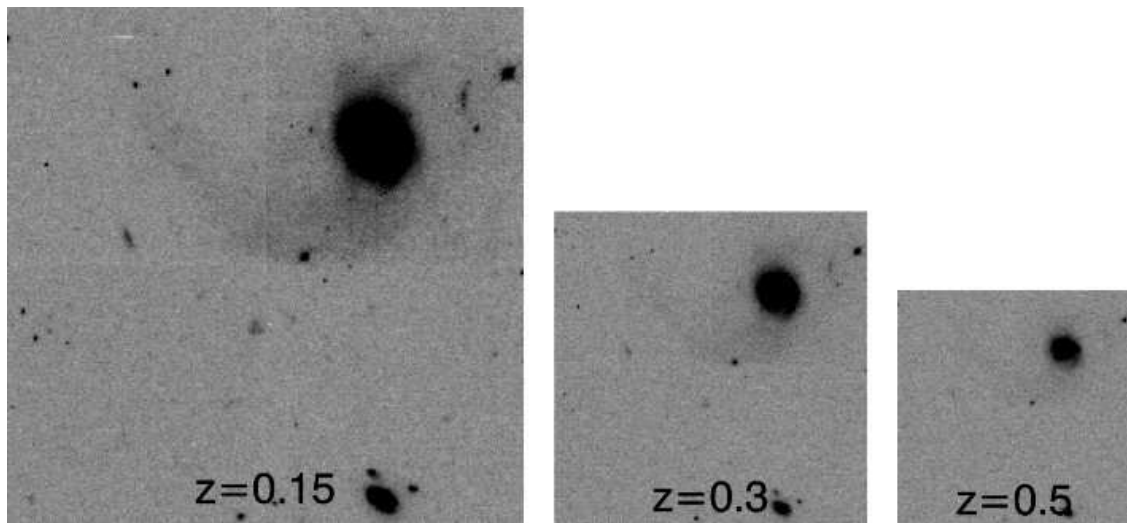
Fig. 11.— Artificially redshifted images of EA3. We rebin the F702W band image of EA3 and fade it artificially to mimic what it would look like at higher redshifts. The rebined images are convolved with the PSF, and then the sky background and noise proportional to the exposure time are added to the redshifted images.